J Mol Model (2013) 19:1325–1338
DOI 10.1007/s00894-012-1683-x

ORIGINAL PAPER

Effects of bidentate coordination on the molecular properties rapta-C based complex using theoretical approach

Adebayo A. Adeniyi · Peter A. Ajibade

Received: 1 September 2012 / Accepted: 6 November 2012 / Published online: 28 November 2012

Abstract In this work several quantum properties including the NEDA and QTAIM are computed on three models of rapta-C complexes using DFT with hybrid functional and basis set with ECP and without ECP. Several interesting correlations within the observed properties and also with the reported experimental behaviors of these complexes including their biological activities are presented. The study shows that the stability of the two complexes with bidentate ligands is associated with their high hydrogen bonding stability and existence of stronger non-covalent metal-ligand bonds. The energy decomposition analysis indicated that inter-atomic interactions in the three forms of rapta-C complexes and their stability are governed by the charge transfer term with significant contributions from polarization and electrostatic terms. The higher stability of complex **1** and **2** over **3** comes from the lower exchange repulsion and higher polarization contributions to their stability which agrees perfectly with the experimental observation. Our results provide insight into the nature of intramolecular forces that influence the structural stability of the three complexes.

Keywords Bidentate ligands · Molecular properties · Rapta-C complexes · Theoretical approach

Introduction

In an effort to discovered novel metal complexes as alternative anticancer agents that will be active as cis-platin and of a lesser side effect, many metal-based complexes especially that of Ru-based have been synthesized [1]. However, there is yet to be any alternative to cis-platin [2]. One typical Ru-based complexes of interest is rapta-C (r=Ru, a=6-arene, pta= 1,3,5-triaza-7-phosphaadamantane and C mean the arene unit is cymene) (Fig. 1) which has been reported to have better anticancer activities than other models of rapta complexes [2] with reduced likelihood of developing resistance because its anticancer effect occur through different molecular pathways [2]. The major drawback however is that rapta-C activities is limited because of premature hydrolysis before getting into the cancer sites which is an indication that it has to be administered in saline to suppress the cleavage of the chloride ligands [3]. Effort to address this limitation led to the synthesis of two other forms of rapta-C called carbo-rapta-C and oxalo-rapta-C (Fig. 1) with bidentate carboxylate ligands which were reported to be a prototype of the structures of carbo-cisplatin and oxalo-cisplatin [4]. Both carbo-and oxalo-rapta-C are reported to resist hydrolysis [4] and have high anticancer activities similar to the parent complex rapta-C. However, oxalo-rapta-C is known to completely resist hydrolysis while carbo-rapta-C can moderately be hydrolyzed [5]. Also, carbo-rapta-C is known to show higher anticancer activity than oxalo-rapta-C [2, 5]. These two complexes containing bidentate ligands are reported stable while their parent complex rapta-C is unstable [3, 5].

Many of the Ruthenium-arene complexes of these types have been reported to be unstable and have complicated ligand exchange chemistry [3]. In drug design there is need for a clear understanding of the physicochemical properties of potential drug candidates [6] which will enhance their rational design. Therefore, it is of prime importance to us to explore the electronic properties of the carbo-rapta-C, oxalo-rapta-C and their parent complex rapta-C (Fig. 1) which have been proposed as anticancer agents. There are many

A. A. Adeniyi · P. A. Ajibade (✉)
Department of Chemistry, University of Fort Hare,
Private Bag X1314,
Alice 5700, South Africa
e-mail: pajibade@ufh.ac.za

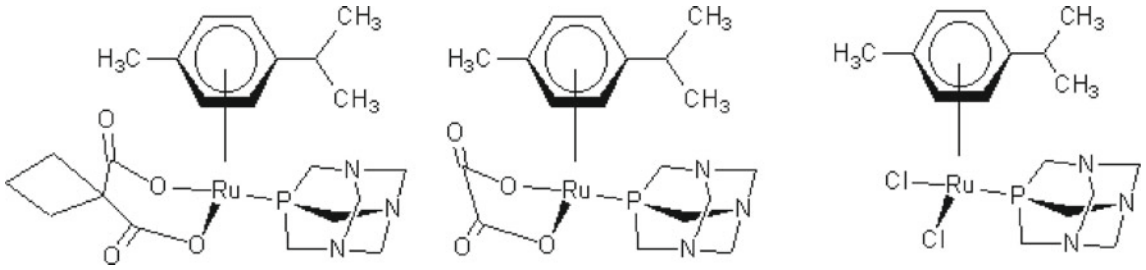

Fig. 1 The schematic structures of complexes **1**, **2** and **3**

experimental reports on the anticancer activities of these metal-based complexes without any detailed understanding of electronic structural properties in relation to the observed activities and the instability of some complexes [3]. We are interested in studying the chemistry of the three models of rapta complexes to understand ways of increasing their stability as a means of getting better drug candidates [3]. We made several efforts where it is possible to relate computed molecular properties to their biological activities and other experimental properties. The computed properties from natural energy decomposition analysis (NEDA) and quantum theory of atoms in molecules (QTAIM) analysis are employed to give possible reasons for the reported higher solubility and stability of oxalo-rapta-C and carbo-rapta-C compare to the precursor rapta-C [5].

Organometallic complexes unlike organic compound are rarely studied computationally due to difficulties of optimizing and computing metal complexes [7]. However, there have been little computational studies on rapta complexes like its application in clarifying the experimental data on pK_a values [8], docking to cancer macromolecules [5], QM/MM study of the interaction of Ru(II)-based complexes to macromolecules [7], and DFT study of the interactions of the complexes with residues that characterize the binding sites of cancer macromolecules [9]. Unfortunately, all the available theoretical studies on these metal-based anticancer complexes lack a real description of the nature and amplitude of the intramolecular interactions that can influence the stability of these complexes.

The goal of this work is to investigate the physicochemical nature of the intramolecular non-bonded forces that determine the stability and also affect the anticancer behavior of the complexes. In order to gain insight into the structural stability of these complexes, we applied natural bond orbital (NBO), natural energy decomposition analysis (NEDA) and quantum theory of atoms in molecules (QTAIM) analysis. Some of the most significant properties of interest are the non-covalent interactions that have been discovered to govern the stability of complexes [10]. Besides hydrogen bonds, the interactions between anions and π-systems have been pointed out to be among the strongest non-covalent interactions which depend on the extent of electron-deficiency of the π-system [10]. Many of these non-covalent properties can be analyzed making use of AIMAll which is a software package for performing quantitative and visual QTAIM analyses of molecular systems starting from molecular wavefunction data [11]. In this package, the nuclear critical points (NCP) correspond to atomic nuclei is the local maxima, or attractors, of electron density that can be connected by a gradient path called the atomic interaction line (AIL) or bond path. AIL corresponds to the line of maximum electron density between the two nuclei and is indicative of chemical bonding between the two atoms. The nature of chemical bonding between two atoms is characterized with bond critical point (BCP) which is the point of minimum electron density along a bond path. The interatomic surfaces (IASs) are the zero-flux surfaces perpendicular to the bond paths at the BCP which formally separate the atoms from each other in molecules. Within the framework of QTAIM, chemical bonding is identified with the presence of bond critical points (BCPs) denoted as (3,-1) CPs between maxima as a necessary and sufficient condition for atoms to be bonded to one another [12].

To the best of our knowledge, this is the first time a comprehensive atomic behavior in these complexes will be discussed. We also discuss important features identified in the theoretical structural analysis of complexes such as non-nuclear attractor (NNA) critical point (CP) which has recently been experimentally confirmed [12, 13]. This feature is known to occur in rare instances where electron density distributions can exhibit a maximum without an associated nucleus at that position.

Computational methods

The computational simulations were done using FIREFLY 7.1.G [14], Gaussian 03 [15] and AIMAll 12.06.03 [11]. Firefly QC package [14], which is partially based on the

GAMESS (US) [16] source code, was used for all the NBO and NEDA analysis. All the optimization of the complexes and some quantum properties were computed using PBE0 hybrid density functional [17] with a mixture of two different external basis sets obtained from EMSL Basis Set Library [18, 19] which were incorporated into the input file in a format that each FIREFLY and Gaussian program can read. The complexes were initially optimized in FIREFLY using a combination of basis set 6-31G which applied valence double zeta (VDZ) and the second basis set SBKJC VDZ [20] with effective core potential (ECP). On atoms of Ru, P and Cl, SBKJC VDZ ECP basis set was applied while the remaining atoms were computed using 6-31G basis set. The second optimization was done using G03 with just a little difference of adding polarization to all heavy atoms except H by using 6-31G* basis set. After the optimization, all other computed properties using G03 and FIREFLY were done at this last combination of basis sets. Many other quantum properties were recomputed in G03 package using B3LYP hybrid functional [21] and all electron basis set 3-21G [22] on the optimized geometries at gas phase of 1 atm and default temperature of 273.15 K. SBKJC VDZ ECP basis set added three s, three p, two d, and one f orbitals for the Ru atom but only two s, two p and one d for other none metals on which the ESP basis set is applied. The choice of SBKJC VDZ ECP basis set with PBE0 is as a result of a large number of electrons and configurations to be treated and due to the past records of their effectiveness in computational study of metal clusters [23, 24] and because it incorporates relativistic corrections for the metal atoms [25]. On each of the molecules, 28 core electrons were removed from Ru (1s, 2s, 2p, 3s, 3p, 3d), 10 from P (1s, 2s, 2p) and 10 from Cl (1s, 2s, 2p) atoms and were treated with pseudo potential while the valence electrons were treated by a double zeta quality functions.

Natural bond orbital (NBO) analysis [26] and natural energy decomposition analysis (NEDA) [27] have been carried out using NBO 5.0G program [28] as implemented in FIREFLY 7.1.G. The charges of each atom were also analyzed on the basis of NPA [29]. The number of electrons transferred from the metal lone pairs to ligand and also from the ligands to metal to the total electrons transferred with stabilization energy greater than 10.00kJ mol^{-1} is reported on the basis of the second order perturbation theory ($E^{(2)}$) analysis. The intensity of the interaction between electron donors and electron acceptors is directly proportional to the value of stability energy of the 2nd-order perturbation $E^{(2)}$. The larger the value of $E^{(2)}$, the more donating tendency from electron donors to electron acceptors and the greater the extent of conjugation of the whole system [30]. This analysis is carried out by examining all possible interactions between "filled" (donor) Lewis-type NBOs and "empty" (acceptor) non-Lewis NBOs, and estimating their energetic importance by 2nd-order perturbation theory.

$$E^{(2)} = \Delta E_{ij} = q_i \frac{F(i,j)^2}{\varepsilon_j - \varepsilon_i}$$

For each donor NBO (i) and acceptor NBO (j), the stabilization energy E(2) associated with delocalization ("2e-stabilization") $i \rightarrow j$ can be estimated, where q_i is the donor orbital occupancy, ε_i, ε_j are diagonal elements (orbital energies) and F (i,j) is the off-diagonal NBO Fock matrix element.

The electron density topology and atomic properties were evaluated within quantum theory of atoms in molecules (QTAIM) using AIMAll. The calculation of the atomic properties was carried out by integration within the atomic basins using little modification to the default parameters. In order to present the complementary characteristics of bonds, the topological properties of the charge density ρ(r) were analyzed through QTAIM approach to determine both the gradient (∇ρ) and the Laplacian of the charge density ($\nabla^2\rho$) [31] as implemented in AIMAll version 12.06.03 [11]. In most cases Proaim method of atomic basin integration was used coupled with a very high basin quadrature that corresponds to uniform and Gauss-Legendre quadratures for the Phi and Theta spherical polar angular coordinates respectively. Other parameters used are fine IAS mesh for adjacent interatomic surface (IAS) paths and outer ang of basin quadrature control set to 3/2.

According to the reported theory of molecular structures by Bader and co-workers [32] which is based on topological properties of electron density ρ(r), using zero-flux surfaces which satisfy the condition that ∇ρ(r).n=0 for every point on the surface of the subsystem where n is a unit vector to the surface, a molecule may be partitioned into atoms [33]. The points on the surfaces which are saddle points in the electron density are referred to as critical points at which the gradient of electron density is zero (∇ρ(r) = 0) [12, 33].

Results and discussion

Natural orbital analysis

The hybridization of Ru(II) metal (Table 1) for all three complexes (Fig. 1) shows that $4d^7$ orbitals are used preferentially

Table 1 Hybridization and Lewis properties in terms of percentage total electron density distribution of the complexes

Molecule	Ru(II) valence rating	Total Lewis	Val non-Lewis	Rydberg non-Lewis
1	4d7 < 5s1	97.536% of 138	2.28%	0.18%
2	4d7< 5s1	97.384% of 123	2.44%	0.18%
3	4d7< 5s1	97.692% of 118	2.17%	0.14%

in complex formation compared to $5s^1$ orbital as the computed occupancy of s-orbital ranges from 0.13 to 0.40 which is far less than one. These further confirm that the 4d orbitals are lower than that of 5s. The natural Lewis structure description in terms of the percentage of total electron density confirms the stability of the complexes at more than 97% Lewis electrons (Table 1). Also, valence non-Lewis orbitals (description of antibonds or electron delocalization) play a relatively important role in the stability of the complexes as it is associated with a relatively significant percentage compared to the extra-valence orbitals (i.e., Rydberg) in the slight departures from a localized Lewis structure model.

The features of the metal-ligand interaction and bonding (Tables 2 and 3) indicate that there is metal to ligand charge transfer (MLCT) in all three complexes. This is evidenced from the asymmetric polarization of the bonding electron in the natural bond orbital (NBO) analysis as shown in Table 2 where bonding electrons are directed toward the ligand atoms. The percentage of the polarization (c_A-squared) on each hybrid which are in parentheses and the polarization coefficient c_A of the bonding metal-ligand atoms (Table 2) show the electrons are more directed toward the ligand atoms. The ligand atoms in bonding with metal atom are characterized with higher c_A and c_A-squared but during the antibonding the electrons are toward the metal atom. This is typical nature of π ligand metal complexes as it has been established that systems with intense intramolecular charge transfer (CT) between metal and ligand (MLCT or LMCT) transitions will be associated with π back-donation in the complexes [34, 35] which usually results in a very large value of hyperpolarizability [34]. Metal complexes are known to posses intense, low energy metal ligand charge transfer (MLCT), ligand metal charge transfer (LMCT), or intraligand charge transfer (ILCT) transitions [36]. The feature of the HOMO and the LUMO in Fig. 2 also shows that the Ru atom and the bidentate ligands dominate the HOMO while the arene moiety which is a π-ligand are predominantly the LUMO which further confirm the electron transfer from metal to arene carbon atoms. This is different from what is obtained in the bidentate complexes in which the HOMO in the monodentate is dominated by the PTA ligand. Making use of NPA analysis to predict the magnitude of electron transfer [37], a broader features of the electronic interaction within the complexes are show from the second order perturbation theory analysis of fock matrix in NBO basis as shown in Table 3 for those ligand atoms that have stability energy ($E^{(2)}$) up to 10 kcal mol^{-1} in direct interaction with metal atom. There is a significant electron transfer from the Ru(II) lone pair into the carbon atoms of arene unit which range from 0.44596e to 0.48942e in the three complexes considered. However, some of the electrons that were transferred into the carbon atoms of the arene ligand also take part again in the back bonding of electrons into the bonding orbitals of the metal-ligand bond especially that of Ru-P and Ru-O bond of the bidentate complexes due to close contact interactions. The number of electrons involved in the back bonding into the antibonding orbitals of metal-ligand bonds ranges from 0.16022e to 0.24037e. It is only in complex **1** that 0.18716 electrons are directly back bonded from the arene carbon into the antibonding lone pair orbital of the metal. In this NPA analysis, the Ru atom interaction with arene C atoms are suggested as adjacent bonded atom (vicinal, "v"), or a more remote ("r") site since each of the three complexes split into two different units made of an arene unit and all other atoms taken as second unit (Table 3).

The strength of these intramolecular interactions obtained using the bond order analysis (Table 4) of ligand atoms that are in direct bonding with metal is in good agreement with the result obtained from the QAIM analysis. The bond order of the metal-ligand atoms are in the order of Ru-Cl > Ru-P > Ru-O > Ru-C where the carbon atoms are from the arene ligand. The highest bond order of Ru-Cl up to 0.967 and lower bond order of Ru-P and Ru-C coupled with the topological analysis done with AIMAll show that the Ru-Cl is a

Table 2 The polarization of the bonding and the antibonding interaction of Ru(II) with ligand atoms

Comp.	Lewis bonding	(c_A-squared) c_A → (c_A-squared) c_A	Non-Lewis antibonding	(c_A-squared) c_A ← (c_A-squared) c_A
1	σ(Ru-P)	(33.77%) 0.5811*→ (66.23%) 0.8138*	σ*(Ru-O)	(66.23%) 0.8138* ← (33.77%) -0.5811*
	σ (Ru-O)	(23.78%) 0.4876* → (76.22%) 0.8731*	σ*(Ru-O)	(76.22%) 0.8731* ← (23.78%) -0.4876*
2	σ (Ru-O)	(21.12%) 0.4595*→ (78.88%) 0.8882*	σ*(Ru-O)	(78.88%) 0.8882* ← (21.12%) -0.4595*
	σ (Ru-O)	(21.12%) 0.4595* → (78.88%) 0.8882*	σ*(Ru-O)	(78.88%) 0.8882* ← (21.12%) -0.4595*
	σ (Ru-P)	(27.65%) 0.5258* → (72.35%) 0.8506*	σ*(Ru-P)	(72.35%) 0.8506* ← (27.65%) -0.5258*
3	σ (Ru-P)	(31.47%) 0.5610*→(68.53%) 0.8278*	σ*(Ru-P)	(68.53%) 0.8278*Ru ← (31.47%) -0.5610*
	σ (Ru-Cl)	(25.01%) 0.5001* → (74.99%) 0.8660*	σ*(Ru-Cl)	(74.99%) 0.8660* ← (25.01%) -0.5001*
	σ (Ru-Cl)	(24.81%) 0.4981* → (75.19%) 0.8671*	σ*(Ru-Cl)	(75.19%) 0.8671* ← (24.81%) -0.4981*

Polarization coefficient c_A is the values with starred superscript and the square of it is the percentage of the NBO (c_A-squared) on each hybrid orbital (in parentheses)

Table 3 The delocalization orbitals with their second perturbation energies ($E^{(2)}$) and the principal delocalizing acceptor orbitals associated with each donor NBO

Comp.	Delocalization of electrons		Delocalization donor orbitals				Delocalization acceptor orbitals		
	Donor → acceptor	$E^{(2)}$ kcal mol^{-1}	Donor	occ	E	Pda	Acceptor	e$^-$ gain	E
1	1. σ (Ru-O) → 14. σ*(C^u=O^u)	15.28	1. σ (Ru – O)	0.91961	-0.40736	14(v)	8. LP*(Ru)	0.18716e	0.62863
	2. LP(Ru) → 10. LP*(C)	22.72	2 LP(Ru)	0.87731	−0.24553	5(r)	10. LP*(C)	0.46262e	−0.16897
	3. LP(Ru) → 9. LP*(C)	22.81	3. LP(Ru)	0.86880	−0.24643	9(r)	11. LP*(C)	0.44596e	−0.15605
	3. LP(Ru) → 11. LP*(C)	16.20	5. LP(C)	0.49558	−0.17000	10(v)	12. σ*(Ru-P)	0.24037e	0.09092
	4. LP(O) → 8. LP*(Ru)	28.12	6. LP(C)	0.47745	−0.15262	11(v)	13. σ*(Ru–O)	0.23514e	−0.02340
	5. LP(C) → 13. σ*(Ru-O)	43.01	7. LP(C)	0.49089	−0.16396	10(v)	14. σ*(C^u =O^u)	0.11939e	0.05793
	6. LP(C) → 12. σ*(Ru-P)	22.70							
	7. LP(C) → 8. LP*(Ru)	10.43							
2	1. σ(Ru-O) →13. σ*(Ru–O)	11.05	1. σ(Ru-O)	0.95924	−0.45566	14(g)	12. σ*(Ru-O)	0.19245e	0.15949
	1. σ (Ru-O) →14. σ*(Ru–P)	16.36	2. σ(Ru-O)	0.95720	−0.45611	14(g)	13. σ*(Ru-O)	0.19124e	0.16517
	2. σ (Ru-O) →12. σ*(Ru-O)	11.16	3. σ(Ru-P)	0.93212	−0.37226	13(g)	14. σ*(Ru-P)	0.16022e	0.37628
	2. σ(Ru–O) →14. σ*(Ru-P)	16.63	4. LP(Ru)	0.87205	−0.24879	11(r)	9. LP*(C)	0.47318e	−0.16517
	3. σ(Ru-P) →12. σ*(Ru-O)	18.88	5. LP(Ru)	0.86829	−0.25044	9(r)	10. LP*(C)	0.46416e	−0.16617
	3. σ(Ru-P)→13. σ*(Ru-O)	19.15	6. LP(C)	0.47536	−0.16503	10(v)	11. LP*(C)	0.46586e	−0.16623
	3. σ(Ru-P) → 14. σ*(Ru-P)	10.82	7. LP(C)	0.48942	−0.17244	8(v)	7. LP(C)	0.48942e	−0.17244
	4. LP(Ru) → 7. LP(C)	10.60	8. LP(C)	0.48061	−0.17301	7(v)	8. LP(C)	0.48061e	−0.17301
	4. LP(Ru) → 11. LP*(C)	20.77							
	5. LP(Ru) → 8. LP(C)	12.47							
	5. LP (3)Ru → 9. LP*(C)	15.31							
	5. LP (3)Ru → 10. LP*(C)	13.19							
	6. LP (1) C →12. σ*(Ru-O)	19.17							
	7. LP (1) C →13. σ*(Ru-O)	22.04							
	8. LP (1) C →12. σ*(Ru-O)	20.45							
3	1. σ(Ru-P) → 13. σ*(Ru-Cl)	19.10	1. σ(Ru-P)	0.93656	−0.37418	13(g)	12. σ*(Ru-P)	0.17416e	0.25537
	1. σ(Ru-P) → 14. σ*(Ru-Cl)	18.99	2. σ(Ru-Cl)	0.96973	−0.35980	12(g)	13. σ*(Ru-Cl)	0.18941e	0.18579
	2. σ(Ru-Cl) → 12. σ*(Ru-P)	15.19	3. σ(Ru-Cl)	0.97066	−0.36016	12(g)	14. σ*(Ru-Cl)	0.18893e	0.19315
	2. σ(Ru-Cl) → 14. σ*(Ru-Cl)	10.97	4. LP(Ru)	0.88393	−0.24641	6(r)	6. LP(C)	0.47037e	−0.16731
	3. σ(Ru-Cl) →12. σ*(Ru-P)	15.34	5. LP(Ru)	0.85983	−0.24181	9(r)	7. LP(C)	0.48229e	−0.17163
	3. σ(Ru-Cl) → 13. σ*(Ru-Cl)	11.19	6. LP(C)	0.47037	−0.16731	8(v)	8. LP(C)	0.47524e	−0.16572
	4. LP(Ru) → 6. LP(C)	14.58	7. LP(C)	0.48229	−0.17163	6(v)	9. LP*(C)	0.46719e	−0.16497
	4. LP(Ru) → 10. LP*(C)	10.36	8. LP(C)	0.47524	−0.16572	6(v)	10. LP*(C)	0.46930e	−0.15866
	4. LP(Ru) → 11. LP*(C)	10.12					11. LP*(C)	0.46202e	−0.15019
	5. LP(Ru) → 7. LP(C)	16.75							
	5. LP(Ru) → 8. LP(C)	11.72							
	5. LP(Ru) → 9. LP*(C)	22.31							
	6. LP(C) → 14. σ*(Ru-Cl)	16.80							
	7. LP(C) →13. σ*(Ru-Cl)	19.99							
	8. LP(C)→ 14. σ*(Ru-Cl)	20.25							

The orbital analyses in the table are defined in terms of donor orbital, acceptor orbital, second perturbation energy or stability energy ($E^{(2)}$ in kcal mol^{-1}), occupancy (occ), principal delocalizing acceptor (Pda), quantity of electron gain (e$^-$ gain) and energy level (E). The topological relationship to the NBO if attached to the same atom (geminal, "g"), to an adjacent bonded atom (vicinal, "v"), or to a more remote ("r") site. The amount of electron loss is calculated on the basis of NPA at the same level. The supercript "u" is on atoms that are not bonded to a metal atom

strong ionic bond while the rest of the metal-ligand bond should be a dative bond. We observed that the strength of the bond order is not in direct relation with the bond distance for the two Ru-Cl in complex 3 which have the highest bond distance and also have the highest bond order (Table 4).

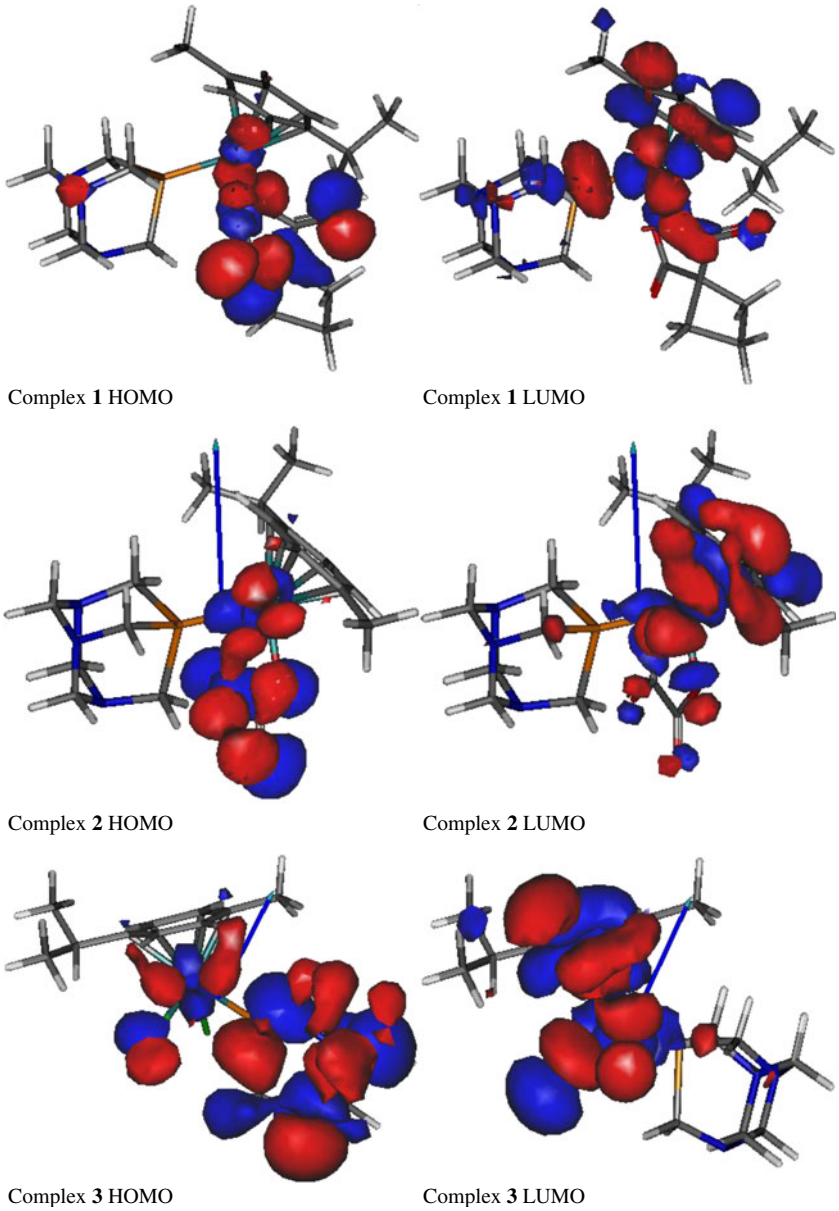

Fig. 2 The HOMO (right) and the LUMO (left) of complexes 1, **2**, and 3 in an ascending order. (3,-1) bond critical points (BCPs) are shown as small green spheres, (3,+1) ring critical points (RCPs) as small red spheres, and (3,+3) cage critical points (CCPs) as small blue spheres and the non-nuclear attractor (NNA) in complex **1** as a large pink sphere. 1a and 1b stand for when ECP basis was used and when all electron minimal basis was used for complex **1**

Natural energy decomposition analysis

In the NEDA calculation, charge transfer (CT) is found to make a significant contribution to the ruthenium-ligand (Ru-L) interaction for all models studied (Table 5). The magnitude of CT is far higher than the electrical interactions which include both the electrostatic (ES) and polarization (POL) contributions. The POL with CT and SE make the largest individual contribution to strong attractions that are necessary for binding to overcome the strong CORE repulsions at the equilibrium geometry of H-bonding (far inside van der Waals contact) resulting in the final net H-bond stabilization energy (E). The results from NEDA analysis show that **1** and **2** have higher hydrogen bond stability (Table 5) than the precursor complex **3** which is the direct effect of their higher polarizabilty than complex **3**. Interestingly also, the feature of the intramolecular interaction of atoms obtained from AIMALL also shows that complex **1** has a higher hydrogen network (Fig. 3 and Table 6) than the other two complexes just as NEDA rated to have the highest hydrogen bond stability (Table 5). This is in good agreement with the reported experimental results where **1** and **2** were found to be highly soluble and more stable than their precursor complex **3** that contains two chloride ligands in place of the carboxylate ligands [5]. Polarizability is a measure of the deformability of the electron density around an atomic or molecular system and it is a key element for describing electronic structure and plays an important role in governing noncovalent interactions [38]. The higher solubility of complexes **1** and **2** should also be the direct effect of their

Table 4 Bond order shows other atoms in the molecule that are interacting with the metal center

	Complex **1**		Complex **2**		Complex **3**	
	Bond length	Bond order	Bond length	Bond order	Bond length	Bond order
Ru-P	2.430	0.590	2.429	0.594	2.420	0.725
Ru-C	2.211	0.439	2.230	0.382	2.231	0.416
	2.233	0.423	2.225	0.390	2.205	0.441
	2.266	0.348	2.232	0.413	2.198	0.446
	2.249	0.429	2.241	0.411	2.205	0.452
	2.213	0.433	2.239	0.429	2.236	0.392
	2.232	0.425	2.231	0.442	2.295	0.332
Ru-Cl			2.500	0.966		
			2.496	0.947		
Ru-O	2.100	0.659	2.090	0.682		
	2.119	0.667	2.086	0.673		

higher intramolecular hydrogen bond (HB) interactions which will enhance their interaction with the polar solvent environment. HB has been described to base on two different effects which are electrostatic field effect and orbital delocalization effect [39].

The NEDA analysis fragmented each of the complexes into two, of which one fragment is the arene ligand ($C_{10}H_{14}$) and the remaining part of the each complex represents the second fragment. The calculated dipole moment for the perturbed (def) and optimized (cp) wavefunctions which can be interpreted as each unit in isolation and in the presence of each other respectively show a relatively significant shift in dipole (i.e., induce dipole). The induce dipole in Debye for 1, **2** and **3** complexes are 1.41, 0.71 and 1.03 respectively for fragment one and 1.47, 1.33 and 1.45 for fragment two. The implication of these significant values of induced dipole is that there is no strict orthogonality required of wavefunctions of the first and second fragments but are both characterized by significant polarization thereby better exposing them as acceptor and donor to nucleophilic and electrophilic attack respectively. The electric dipole moment of a molecule is the first derivative of energy with respect to an applied electric field and it is the measurement of the asymmetric in molecular charge distribution. We observed that the induced dipole values of complexes **1** and **3** are higher than complex **2** which can be the reason while complex **1** is often experimentally found to be an active anticancer like complex **3** [2, 5] possibly because of better expose surface for macromolecular attack. In addition, this could be the reason while complex **2** is found to completely resist hydrolysis compared to complexes **1** and **3** [5]. Also, the two fragments of each complex act synergistically with each other as we found that the difference between the energy of localized ψA(def) and optimized ψA (cp) for the three complexes considerably improved. The synergistic effect of the fragment favors the stability of the arene fragment in the three complexes (−0.83,−0.80 and−0.78 a.u) above the second fragment (−0.50,−0.49 and−0.52 a.u). Likewise, we can suggest that the synergistic effects from metal and ligand can lead to highly cytotoxic species as it was experimentally suggested [40].

Atoms in molecules analysis using B3LYP/3-21G functional

The atoms in molecules analysis of the complexes using AIMAll confirmed the presence of both strong and weak noncovalent interactions. In interpreting the features of the quantum theory of atoms in molecules (QTAIM) topology, the critical points density ($\nabla\rho$) gives information about the existence of bonds, while the sign of Laplacian of the density ($\nabla^2\rho$) at that point reflects the kind of interaction which if it is negative is a critical point for covalent interactions (open shells), and if it is positive is a closed shell interaction, such as hydrogen bonds [31] or ionic or van der Waals bond [41]. The Laplacian features of each complex electron density ($\nabla^2\rho$) are shown using the contour plot along the plane of the P, Ru and Cl or O in the bidentate complexes (Fig. 3) and many of the atoms of the complexes are found on the chosen plane. All the ligand-ligand bonds are characterized with negative $\nabla^2\rho$ (dash lines) whiles the metal-ligand bonds are characterized with positive $\nabla^2\rho$ (solid lines) which further confirmed that they are covalent and non-covalent interactions respectively. The QTAIM topological features of the three complexes show that the

Table 5 The summary of the natural energy decomposition analysis showing the components of interaction energy in kcal mol^{-1}

Comp.	CT	ES	POL	XC	DEF	SE	Electrical	Core	E
1	−402.36	−157.67	−169.20	−176.52	834.49	82.1	−244.77	575.87	−71.26
2	−1079.81	−151.05	−162.92	512.35	810.4	78.58	−235.39	1244.16	−71.04
3	−819.55	−162.03	−133.42	28.28	818.81	63.52	−231.93	983.58	−67.90

The components of energy are defined in terms of charge transfer (CT), electrostatic interaction (ES); polarization (POL); electrical self-energy (SE); exchange interaction (XC); deformation energy (DEF), electrical (ES+POL+SE), core (XC+DEF-SE) and total interaction energy which is the final net H-bond energy (E = electrical + core + CT)

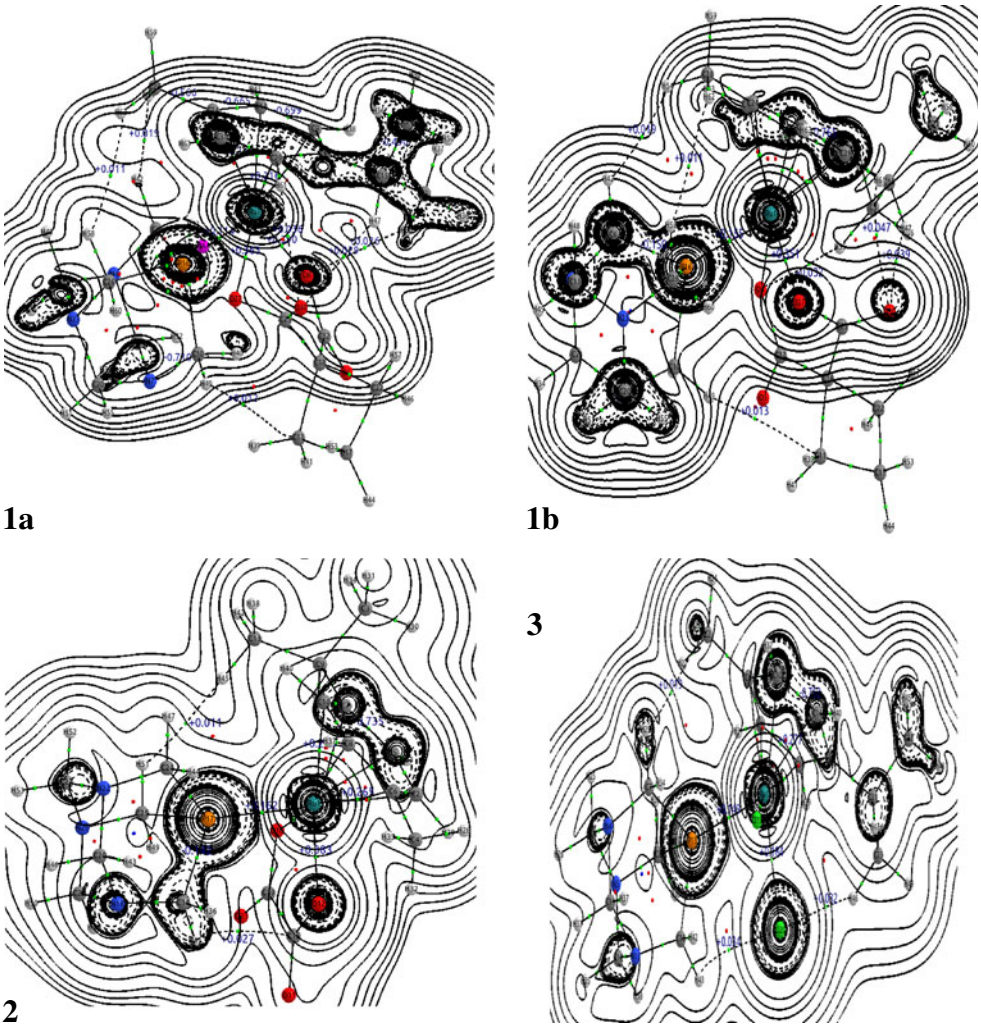

Fig. 3 Laplacian of the electron density in a plane containing P, Ru and Cl or O nuclei (positive contours as solid and negative contours as dashes lines are drawn from 0 to ±800) and bonds (strong bonds in solid and HB in dash lines) for complexes **1**, **2** and **3**

complexes are significantly different from each other due to different networks of hydrogen bonds (HB). The three complexes have 6 RCPs in the arene ligand, 4 RCPs in pta and 1 CCP at pta except for complex 3 that have 5 RCPs because the bonding with the last carbon of arene was stretched. Peculiar to complex 1, there are extra 6 RCPs for each of the six HB ring but 1 RCP for the bidentate unit against expected 2 which is due to complex HB formed as show in Fig. 3 (1b). Also, complex 2 has 1 RCP for the bidentate unit and 2 RCPs for the two HB while 1 has 3RCPs for the three HB ring formed.

The typical nature of covalent bond which is an open shell interaction is a higher negative value of $\nabla^2\rho(r)$, higher $\rho(r)$ value, low kinetic energy per electron and higher magnitude of the ratio of potential to kinetic energy (V/G) [12]. The covalent bonds have higher negative values of V, high $\rho(r)$, higher negative values of $\nabla^2\rho(r)$, higher negative value of V/G and lower kinetic G. The $\nabla^2\rho$ values for the BCP of M-L bonds are positive but far higher than that of exiting hydrogen bonds (HB) which are characterized with low +ve value of $\nabla^2\rho$ as shown in (Table 6). The high +ve $\nabla^2\rho$ values of BCP for M-L and the corresponding high values of $\rho(r)$ is an indication of strong non-covalent bonds [41]. This gives the reason why the bond order for M-L bonds are relatively (Table 4) low except for Ru-Cl bond of complex **3** that is suggested to be an ionic bond. This supports the NBO analysis that indicates d-orbitals of the metal as the highest occupied molecular orbital (HOMO) of the model system which carries the highest percentage in bonding to ligand atoms. Also, the topological features in Table 6, further confirm the reason while complexes **1** and **2** containing bidentate ligands are experimentally reported to resist hydrolysis more than complex **3** [4] and the reason why **2** completely resists hydrolysis compared to **1** [5]. These properties are suggested to be the result of a stronger non-covalent bond of the Ru-O bonds of the bidentate ligand which is characterized with the highest $\rho(r)$ and $\nabla^2\rho(r)$ compared to other Ru-ligand bonds. Moreover, complex **2** appears to have higher $\rho(r)$ and $\nabla^2\rho(r)$ than complex **1** and the two Ru-O bonds are almost the same while a bigger difference exists between the two Ru-O bonds of

Table 6 Electron density critical point analysis of selected bonds in complex **1, 2,** and **3**

	Bonds	ρ(r)	$\nabla^2\rho$	Ellipticity	K	BPL-GBL_I	V	G	L	V/G
a. Complex **1**										
pta	Ru1-P16	0.073	0.155	0.186	0.017	0.011	−0.072	0.055	−0.039	−1.300
arene	Ru1-C9	0.077	0.265	0.214	0.011	0.010	−0.089	0.078	−0.066	−1.146
	Ru1-C14	0.071	0.291	1.009	0.008	0.029	−0.089	0.081	−0.073	−1.098
	Ru1-C19	0.068	0.277	2.574	0.007	0.027	−0.083	0.076	−0.069	−1.091
	Ru1-C24	0.072	0.256	0.400	0.009	0.013	−0.083	0.073	−0.064	−1.129
	Ru1-C31	0.071	0.295	1.647	0.007	0.046	−0.088	0.081	−0.074	−1.088
	Ru1-C29	0.077	0.262	0.331	0.011	0.010	−0.089	0.077	−0.066	−1.149
bidentate	Ru1-O8	0.086	0.379	0.215	0.011	0.005	−0.118	0.106	−0.095	−1.107
	Ru1-O27	0.083	0.351	0.296	0.012	0.001	−0.112	0.100	−0.088	−1.121
HB	O8-H35	0.006	0.032	0.259	−0.002	0.009	−0.004	0.006	−0.008	−0.627
	C11-H49	0.003	0.013	1.235	−0.001	0.028	−0.002	0.003	−0.003	−0.723
	O30-H47	0.008	0.039	0.090	−0.002	0.016	−0.005	0.007	−0.010	−0.687
	H42-H54	0.005	0.019	0.213	−0.001	0.026	−0.002	0.003	−0.005	−0.608
	H58-H62	0.003	0.011	0.603	−0.001	0.133	−0.001	0.002	−0.003	−0.681
	O30-H61	0.010	0.047	0.672	−0.002	0.096	−0.007	0.009	−0.012	−0.739
b. Complex **2**										
pta	Ru1-P17	0.073	0.162	0.166	0.016	0.010	−0.073	0.057	−0.041	−1.287
arene	Ru1-C2	0.073	0.281	0.767	0.009	0.017	−0.088	0.079	−0.070	−1.114
	Ru1-C6	0.074	0.265	0.397	0.010	0.016	−0.086	0.076	−0.066	−1.129
	Ru1-C5	0.074	0.274	0.561	0.010	0.015	−0.088	0.078	−0.069	−1.125
	Ru1-C7	0.072	0.272	0.627	0.009	0.023	−0.085	0.077	−0.068	−1.113
	Ru1-C10	0.073	0.274	0.414	0.009	0.018	−0.087	0.078	−0.068	−1.121
	Ru1-C8	0.071	0.282	0.865	0.008	0.027	−0.087	0.079	−0.071	−1.103
bidentate	Ru1-O12	0.090	0.383	0.194	0.013	0.003	−0.122	0.109	−0.096	−1.121
	Ru1-O16	0.091	0.386	0.196	0.013	0.004	−0.123	0.110	−0.096	−1.122
HB	C15-H41	0.007	0.027	1.073	−0.001	0.057	−0.004	0.005	−0.007	−0.740
	H45-H51	0.003	0.011	0.200	−0.001	0.015	−0.001	0.002	−0.003	−0.572
c. Complex **3**										
pta	Ru1-P13	0.076	0.149	0.143	0.018	0.008	−0.073	0.055	−0.037	−1.327
arene	Ru1-C6	0.074	0.278	0.691	0.010	0.017	−0.089	0.079	−0.070	−1.121
	Ru1-C9	0.077	0.290	0.425	0.011	0.017	−0.094	0.083	−0.072	−1.130
	Ru1-C10	0.077	0.282	0.266	0.012	0.014	−0.094	0.082	−0.071	−1.141
	Ru1-C14	0.077	0.269	0.263	0.012	0.013	−0.091	0.079	−0.067	−1.149
	Ru1-C16	0.072	0.277	1.380	0.008	0.030	−0.086	0.077	−0.069	−1.106
mono	Ru1-Cl19	0.056	0.182	0.203	0.005	0.002	−0.055	0.050	−0.046	−1.094
	Ru1-Cl20	0.056	0.184	0.169	0.005	0.001	−0.056	0.051	−0.046	−1.095
HB	C2-H29	0.006	0.019	0.854	−0.001	0.121	−0.003	0.004	−0.005	−0.768
	Cl20-H43	0.010	0.034	0.911	−0.001	0.113	−0.006	0.007	−0.009	−0.814
	Cl20-H46	0.010	0.032	0.043	−0.001	0.006	−0.005	0.007	−0.008	−0.775

The parameters that are denoted with "/" shows they are in correlation with every other parameters that are in that row except where "/" appears again. ρ(r) is electron density, $\nabla^2\rho$ is the Laplancian of ρ(r), BPL – GBL_I is bond strain, V is virial field (potential energy density), G is Lagrangian form of kinetic energy density, K is hamiltonian form of kinetic energy density, L (i.e., K – G) is lagrangian density which is (-1/4) $\nabla^2\rho$ while "Ratio" is V/G, i.e., PE/KE (the higher its magnitude the stronger the bond)

complex **1** which may create an imbalance that will permit the hydrolysis. Also, the feature of the Lewis bonding and non-Lewis antibonding in Table 2 shows that one of the Ru-O bonds is missing for complex **1** and the bond order in Table 4 also shows that the Ru-O bonds of complex **1** are associated with a longer unequal bond which will further enhance its hydrolysis compared to **2**.

The correlation of the computed bond properties

The relationship that exists between the computed bond properties can be comprehended using the correlation Table 7 that is constructed over all existing bonds in the three complexes. From this table, high values of ρ(r) should have a high negative value of $\nabla^2\rho(r)$ except where there is a stronger non-covalent bond as in M-L bonds. The values of $\nabla^2\rho(r)$ appear to be strongly related with the values of V/G which is an indication that a stronger bond should be characterized with stronger potential energy density than Lagrangian form of kinetic energy density. A very flat electron density region that is usually characterized with very low average values for ρ(r) and $\nabla^2\rho(r)$ are usually found to have a relatively high ellipticity [42] which can be interpreted as ellipticity is inversely proportional to ρ(r) and negative values of $\nabla^2\rho(r)$. The correlation of the ellipticity of all the bonds in the three complexes with ρ(r) and negative $\nabla^2\rho(r)$ shows that it is inversely proportional and averagely high. The correlation values of ellipticity with ρ(r) as shown in Table 7 are −0.57, −0.72 and −0.65 while with the negative values of $\nabla^2\rho(r)$ are 0.57, 0.65 and 0.60 for complexes **1**, **2** and **3** respectively. The implication is that a high negative value $\nabla^2\rho(r)$ and high positive values of ρ(r), which is a picture of strong open shell covalent bond, are characterized with lower ellipticity while the closed shell interactions of low positive $\nabla^2\rho(r)$, as in HB, are characterized with higher ellipticity. Therefore the Ru-ligand bonds (Table 6) are characterized with higher ellipticity than covalent bonding within the ligands which is a further indication that the metal-ligand bonds are closed shell interactions. The higher ellipticity values of the ruthenium monodentate bonds in complex **3** and ruthenium bidentate bonds in complexe **1** than complex **2** further supports the reported hydrolysis of complexes **1** and **3** while complex **2** completely resists hydrolysis [4, 5]. Also, bonds with relatively high ellipticity are those with higher bond stretching (BPL-GBL_I) with correlation of 0.51, 0.93 and 0.74 in complexes **1**, **2**, and **3** respectively (Table 6).

The intra-atomic properties of the complexes

As expected for all the heavy atoms with largely core electrons, the population of each atom is highly localized (Table 8) while electron density of all the H atoms is strongly delocalized and therefore can easily be perturbed by external influences such as an electric field [12]. The

Table 7 The correlation in the properties of the electron density critical point analysis of complexes **1**, **2** and **3**

ρ(r)#	$\nabla^2\rho$	Ellipticity	K	BPL.GBL_I	V	G	L	Ratio
1	−0.85	−0.57	0.96	−0.62	−0.86	0.39	0.85	−0.71
2	−0.83	−0.72	0.96	−0.74	−0.83	0.36	0.83	−0.64
3	−0.92	−0.65	0.98	−0.60	−0.95	0.23	0.92	−0.80
$\nabla^2\rho$#	Ellipticity	K	BPL.GBL_I	V	G	L	Ratio	
1	0.57	−0.81	0.47	0.54	0.09	−1.00	0.90	
2	0.65	−0.76	0.62	0.45	0.16	−1.00	0.88	
3	0.60	−0.95	0.43	0.82	0.13	−1.00	0.90	
Ellipticity#	K	BPL.GBL_I	V	G	L	Ratio		
1	−0.53	0.51	0.41	−0.06	−0.57	0.48		
2	−0.62	0.93	0.46	−0.07	−0.65	0.57		
3	−0.61	0.74	0.56	−0.05	−0.60	0.55		
K#	BPL.GBL_I	V	G	L	Ratio			
1	−0.53	−0.93	0.51	0.81	−0.60			
2	−0.62	−0.92	0.52	0.76	−0.50			
3	−0.51	−0.96	0.19	0.95	−0.77			
BPL.GBL_I#	V	G	L	Ratio	V#	G	L	Ratio
1	0.46	−0.20	−0.47	0.48	**1**	−0.79	−0.54	0.31
2	0.49	−0.13	−0.62	0.57	**2**	−0.81	−0.45	0.16
3	0.55	−0.29	−0.43	0.44	**3**	−0.46	−0.82	0.59
G#	L	Ratio	L#	Ratio				
1	−0.09	0.29	**1**	−0.90				
2	−0.16	0.40	**2**	−0.88				
3	−0.13	0.37	**3**	−0.90				

The parameters that are denoted with "#" shows they are in correlation with every other parameters that are in that row except where "#" appears again

Table 8 Selected atomic properties derived through the quantum theory of atoms in molecules analysis for complexes **1, 2,** and **3,**

	Name	q(A)	L(A)	K(A)	K_Scaled(A)	Mu_Intra(A)	Mu_Bond(A)	Mu(A)	N(A)	%Loc(A)	%Deloc(A,A')	Vol(A), 0.001
a. Complex **1**												
	Ru1	0.86	9.73E-04	4402.36	−4426.58	0.30	1.64	1.34	43.14	94.18	5.82	98.66
arene	C9	−0.11	−4.40E-05	37.63	−37.83	0.22	0.20	0.21	6.11	65.89	34.11	72.17
	C14	−0.14	4.30E-05	37.62	−37.83	0.24	0.11	0.17	6.14	65.99	34.01	76.94
	C19	−0.08	7.00E-06	37.63	−37.83	0.21	0.40	0.59	6.08	64.89	35.11	59.57
	C24	−0.10	−1.72E-04	37.62	−37.83	0.09	0.27	0.18	6.10	64.87	35.13	61.55
	C29	−0.12	-1.13E-04	37.65	−37.85	0.26	0.36	0.62	6.12	66.00	34.00	71.17
	C31	−0.12	4.70E-05	37.62	−37.83	0.25	0.18	0.23	6.12	65.96	34.04	76.32
pta	P16	0.89	2.52E-04	338.04	−339.90	1.03	0.56	1.59	14.11	86.02	13.98	102.66
Bidentate	O8	−0.95	−7.00E-06	74.55	−74.96	0.13	0.79	0.85	8.95	86.36	13.64	93.88
	O27	−0.95	1.75E-04	74.54	−74.95	0.17	1.01	1.14	8.95	86.87	13.13	96.01
b. Complex **2**												
	Ru1	0.85	−1.02E-04	4402.39	−4426.23	0.37	1.83	1.65	43.15	94.12	5.88	99.40
arene	C2	−0.11	−1.10E-04	37.62	−37.82	0.24	0.18	0.10	6.11	65.99	34.01	75.24
	C5	−0.12	−1.64E-04	37.63	−37.83	0.22	0.16	0.11	6.12	65.92	34.08	73.72
	C6	−0.07	−1.78E-04	37.61	−37.82	0.16	0.30	0.16	6.07	64.86	35.14	61.43
	C7	−0.08	−3.30E-05	37.63	−37.83	0.19	0.20	0.05	6.08	64.80	35.20	58.62
	C8	−0.14	−8.80E-05	37.62	−37.82	0.22	0.11	0.14	6.14	65.93	34.07	76.13
	C10	−0.15	−6.10E-05	37.62	−37.83	0.20	0.10	0.13	6.15	65.89	34.11	74.16
pta	P17	0.82	−3.60E-05	338.07	−339.90	1.05	0.21	1.18	14.18	85.99	14.01	106.82
Bidentate	O12	−0.92	1.64E-04	74.54	−74.95	0.14	0.97	1.05	8.92	86.23	13.77	95.79
	O16	−0.92	1.57E-04	74.54	−74.95	0.15	1.02	1.10	8.92	86.23	13.77	96.49
c. Complex **3**												
	Ru1	0.64	−7.21E-04	4402.59	−4424.39	0.37	1.39	1.48	43.36	94.05	5.95	107.89
arene	C6	−0.09	−2.56E-04	37.62	−37.80	0.12	0.17	0.05	6.09	64.84	35.16	61.85
	C9	−0.13	-1.78E-04	37.62	−37.81	0.23	0.11	0.14	6.13	65.90	34.10	74.95
	C10	−0.11	−3.14E-04	37.63	−37.81	0.24	0.17	0.10	6.11	65.85	34.15	73.23
	C14	−0.12	−1.86E-04	37.63	−37.81	0.23	0.18	0.09	6.12	65.84	34.16	71.88
	C16	−0.12	−1.28E-04	37.63	−37.81	0.23	0.18	0.11	6.12	65.87	34.13	72.90
	C17	−0.06	4.70E-05	37.61	−37.80	0.19	0.05	0.15	6.06	64.88	35.12	59.93
pta	P13	0.86	−2.50E-05	338.02	−339.70	1.02	0.11	0.96	14.14	85.74	14.26	99.49
mono	Cl19	−0.58	9.80E-05	456.63	−458.89	0.14	1.40	1.54	17.58	96.71	3.29	237.25
	Cl20	−0.57	7.60E-05	456.63	−458.89	0.14	0.66	0.79	17.57	96.55	3.45	231.48

q(A) is net charge of atom A, L(A) is Lagrangian of atom A, N(A) is average number of electrons in atom A, K(A) is electronic kinetic energy of atom A (Hamiltonian form), %Loc(A) is percentage of average number of electrons localized in atom A, K_Scaled(A) is approximation to virial-based total energy of atom A, Mu_Intra(A) is magnitude of intraatomic dipole moment of atom A, Ee(A) is contribution of atom A to electronic energy of molecule, %Deloc(A,A') is the percentage of electron delocalization index of atom A and Vol(A) is the volume bounded by an isosurface of the electron density distribution (0.001) and by interatomic surfaces of atom A

properties of some of the selected atoms of interest which are directly bonded to Ru metal are shown in Table 8. All the atomic basins have integrated Laplacian values L(A) of approximately equal to zero (Table 8), indicating satisfactory numerical integration [12]. As clearly shown in Table 8, the arene carbon atoms become more electronegative as a result of MLCT. The complex HB bonds network observed in the complexes as shown in Fig. 3, are a direct consequence of one centeer being more electronegative than the other as the atoms that are involved in HB are of different atomic charges (Table 8). We observed from the correlation of the atomic properties obtained for all the atoms in the complexes that the number of localized electrons Loc(A) on each atom has a highly direct relation with kinetic energy K (A) (0.91, 0.91 and 0.89), dipole of each atoms use in bonding (Mu_bond) (0.75, 0.76 and 0.80) and volume of the electron density on each atom using the isosurface of 0.001 (0.67, 0.67 and 0.67) in complexes **1**, **2** and **3** respectively as

given in parenthesis. This Loc(A) is also has a high inverse relation with virial energy scaled (K_Scale) (−0.91,−0.91 and−0.89) and percentage of delocalized electrons (−0.71, −0.70 and −0.77) for complexes **1**, **2** and **3** respectively. We observed that Cl, Ru and P in descending order have the highest density volume V(A) as in Table 8 which consequently resulted to their lower ρ(r) and $\nabla^2\rho(r)$ bond interaction for the Ru-Cl and Ru-P bonds (Table 6a–c) that involve the interaction of two atoms of large V(A). The atomic volume V(A) of Ru atom is found to be higher in complex **3** compared to complexes **1** and **2** which can possibly enhance its better hydrolysis and anticancer activities.

Taking a critical look at the molecular sum over of the atomic properties for complexes **1**, **2**, and **3**, we observed that the total K(A) are 6045.16, 5891.34 and 6432.41 while the total V(A) are 3603.91, 3116.36 and 3069.81. It is interesting to point out that the higher total values of K(A) of complexes **3** and **1** over complex **2** is in the order of their reported anticancer activities [2].

Atoms in molecules analysis using PBE0/6-31G*(SBKJC VDZ ECP) functional

When ECP basis set was applied on P, Ru and Cl atoms where applicable, the intramolecular features in QTAIM topology shows that there is non-nuclear attractor (NNA) critical point (CP), i.e., (3,−3) CP but this NNA disappeared when all electron basis set was applied on the three complexes. A typical feature for complex **1** is shown in Fig. 3 as **1a** and **1b** when ECP basis set and all electron basis set were used respectively. In making use of the ECP, even though we obtained similar features when all electron basis set was used yet there is a higher number of RCPs because of the introduction of NNA into complex 1a (pink sphere in Fig. 3(1a)). The computed feature of the topology when the ECP was applied on Ru and P atoms shows that there is a common NNA between the Ru-P bond in the three complexes which is very close to P atom characterized with $\nabla^2\rho$ of 3.22, 3.22 and 3.18 for P-NNA bond and 0.11, 0.12 and 0.11 for NNA-Ru bond in complexes **1**, **2** and **3** respectively. The higher values of $\nabla^2\rho$ for P-NNA and lower for NNA-Ru is an indication that the electronic configuration of metal atom was well represented with the ECP basis set. Also, the contour plot in Fig. 3 for complex 1a shows that the NNA is within the negative contour (dash lines) around P atom which further confirms that the NNA was introduced to compensate for the deficiency of electrons around P due to application of ECP. Therefore, in computing molecular properties it may be proper to limit the application of ECP to metal atom only. The $\nabla^2\rho$ at the NNA is positive like every other observed metal to ligand atomic bond, indicating the local depletion of electron density. In complex **3** where extra ECP was applied on the two Cl atoms, we observed four additional NNA with two NNA allocated to each Cl atom. There have been several discussions on the observation of NNA which are very controversial. It was shown that NNA feature is not just an artefact of computational methods but a genuine feature of the electron density distribution of some complexes [13] and an instance of the first unambiguous experimental evidence of such a feature in a stable molecule has been reported [12]. The experimental evidence of the presence of NNA was done using advanced multipole model to reproduce the calculated electron density distributions (EDD) where a significantly negative value of Laplacian was observed for the presence of a NNA, or (3,-3) CP close to the midpoint of the Mg-Mg internuclear vector was observed [12]. NNA is otherwise referred to as pseudoatoms and was reported to be remnants of or portions of atoms that are not perturbed enough in a molecule in order to remove an essential atomic characteristic [33]. It was further reported to originate from the shape of valence molecular orbitals and might occur in bonds of low polarity in which core contributions are negligible and the radial form of the valence orbitals dominates the total density [12, 33]. There have been many theoretical calculations that strongly suggest that NNAs should be a feature in some metal-metal bonds [12]. The presence of a NNA and associated pseudoatom for the chemistry and physics of molecules has been pointed out as a fascinating area that is ripe for further study [12]. However, based on our observation of NNAs that were present in the ECP basis set computation disappeared when all electron basis set was used is indication that this is a consequence of insufficiency of pseudo potential of ECP to completely account for the electrons around some atoms which were computationally compensated for through the introduction of NNA. Even though our observed NNA was suggested to be far from integration error as the values of the calculated Lagrangian of atom L(A) is close to zero (0.015 and-0.011 for complexes **1** and **2** respectively) and the bond paths are not associated with low values of ρ(r) and $\nabla^2\rho(r)$ that would have been interpreted with care [42], yet it cannot be suggested to be real since it disappeared when all electron basis set was used. This finding is close to what was discussed on the observation of NNA which turned out to be a mere artefact of an inappropriate basis set [13]. Also, close to our observation is the reported larger extension of the core density of sodium compared to lithium which efficiently quenches the existence of a NNA in sodium, while for Li the core is sufficiently contracted to allow for the creation of a NNA [12].

Conclusions

In this work we have been able to show strong correlation of the quantum properties of complexes **1**, **2** and **3** with their

reported varying stability, hydrolysis and anticancer activities. An insight into the molecular properties like NBO, NEDA and QTAIM analysis of these three Ru-based complexes are provided using DFT method. From the NBO analysis, we observed that the three systems are characterized mainly with MLCT specifically from the Ru atom to the lone pair C atoms of π-ligand arene. The NEDA analysis shows the most significant factor that determines the stability of the complexes is charge transfer followed by strong polarization and electrostatic. There is a high synergistic effect of the metal coordinated ligands on each other resulted in high induced dipole and induced stabilization energy which further supports the reported differences in their stability and anticancer activities. The QTAIM analyses show that the metal-ligand bonds are characterized with non-covalent bonds which are suggested to be dative-covalent except for the Ru-Cl suggested to be an ionic bond. We equally found out that the presence of NNA in our system with ECP basis set is complete computational artefacts which suggest the application of ECP will be appropriate in computing intramolecular properties if limited to metal atoms only in these complexes. In addition to the significant effect of the bonds $\rho(r)$ and $\nabla^2\rho(r)$, bond ellipticity and the ratio of the potential energy density and Lagrangian form of kinetic energy density (V/G) are found to significantly influence the reported differences in the hydrolysis of the complexes. The intra-atomic properties computed show that the atomic electrons are largely localized except for the H atoms which are highly delocalized and can be easily perturbed. The atomic volume V(A) of the Ru atom is found higher in complex **3** than complexes **1** and **2** which can further enhance its reported higher hydrolysis and anticancer activities.

Acknowledgments The authors gratefully acknowledged the financial support of Govan Mbeki Research and Development Centre, University of Fort Hare, South Africa.

References

1. Hartinger CG, Jakupec MA, Zorbas-Seifried S, Groessl M, Egger A, Berger W, Zorbas H, Dyson PJ, Keppler BK (2008) KP1019, a new redox-active anticancer agent—preclinical development and results of a clinical phase I study in tumor patients. Chem Biodivers 5:2140–2155
2. Chatterjee S, Kundu S, Bhattacharyya A, Hartinger CG, Dyson PJ (2008) The ruthenium(II)–arene compound RAPTA-C induces apoptosis in EAC cells through mitochondrial and p53–JNK pathways. J Biol Inorg Chem 13:1149–1155
3. Allardyce CS, Dorcier A, Scolaro C, Dyson PJ (2005) Development of organometallic (organo-transition metal) pharmaceuticals. Appl Organometal Chem 19:1–10
4. Gasser G, Ott I, Metzler-Nolte N (2011) Organometallic anticancer compounds. J Med Chem 54:3–25
5. Ang WH, Daldini E, Scolaro C, Scopelliti R, Juillerat-Jeannerat L, Dyson PJ (2006) Development of organometallic ruthenium−Arene anticancer drugs that resist hydrolysis. Inorg Chem 45:9006–9013
6. Pratuangdejkul J, Pascale Jaudon P, Ducrocq OC (2006) Cation-π interactions in serotonin: conformational, electronic distribution, and energy decomposition analysis. J Chem Theory Comput 2:746–760
7. Ciancetta A, Genheden S, Ryde U (2011) A QM/MM study of the binding of RAPTA ligands to cathepsin B. J Comput Aided Mol Des 25:729–742
8. Gossens C, Dorcier A, Dyson PJ, Rothlisberger U (2007) pKa estimation of ruthenium(II)-Arene PTA complexes and their hydrolysis products via a DFT/continuum electrostatics approach. Organometallics 26:3969–3975
9. Deubel DV, Lau JK (2006) In silico evolution of substrate selectivity: comparison of organometallic ruthenium complexes with the anticancer drug cisplatin. Chem Commun 23:2451–2453
10. Alkorta I, Blanco F, Elguero J, Dobado JA, Ferrer SM, Vidal I (2009) Carbon · · · Carbon weak interactions. J Phys Chem A 113:8387–8393
11. Keith TA (2012) AIMAll (Version 12.06.03), TK Gristmill Software, Overland Park KS, USA, (aim.tkgristmill.com)
12. Platts JA, Overgaard J, Jones C, Iversen BB, Stasch A (2011) First experimental characterization of a non-nuclear attractor in a dimeric magnesium(I) compound. J Phys Chem A 115:194–200
13. Timerghazin QK, Rizvi I, Peslherbe GH (2011) Can a dipole-bound electron form a pseudo-atom? An atoms-in-molecules study of the hydrated electron. J Phys Chem A 115:13201–13209
14. Granovsky AA Firefly version 7.1.G, www http://classic.chem.msu.su/gran/firefly/index.html
15. Frisch MJ, Trucks GW, Schlegel HB, Scuseria GE, Robb MA, Cheeseman JR, Montgomery JA Jr, Vreven T, Kudin KN, Burant JC, Millam JM, Iyengar SS, Tomasi J, Barone V, Mennucci B, Cossi M, Scalmani G, Rega N, Petersson GA, Nakatsuji H, Hada M, Ehara M, Toyota K, Fukuda R, Hasegawa J, Ishida M, Nakajima T, Honda Y, Kitao O, Nakai H, Klene M, Li X, Knox JE, Hratchian HP, Cross JB, Adamo C, Jaramillo J, Gomperts R, Stratmann RE, Yazyev O, Austin AJ, Cammi R, Pomelli C, Ochterski JW, Ayala PY, Morokuma K, Voth GA, Salvador P, Dannenberg JJ, Zakrzewski VG, Dapprich S, Daniels AD, Strain MC, Farkas O, Malick DK, Rabuck AD, Raghavachari K, Foresman JB, Ortiz JV, Cui Q, Baboul AG, Clifford S, Cioslowski J, Stefanov BB, Liu G, Liashenko A, Piskorz P, Komaromi I, Martin RL, Fox DJ, Keith T, Al-Laham MA, Peng CY, Nanayakkara A, Challacombe M, Gill PMW, Johnson B, Chen W, Wong MW, Gonzalez C, Pople JA (2003) Gaussian, Inc., Pittsburgh PA
16. Schmidt MW, Baldridge KK, Boatz JA, Elbert ST, Gordon MS, Jensen JH, Koseki S, Matsunaga N, Nguyen KA, Su S, Windus TL, Dupuis M, Montgomery JA (1993) Gamess (US). J Comput Chem 14:1347–1363
17. Adamo C, Barone V (1999) Toward reliable density functional methods without adjustable parameters: the PBE0 Model. J Chem Phys 110:6158–6170
18. Feller DJ (1996) The role of databases in support of computational chemistry calculations. Comp Chem 17(13):1571–1586
19. Schuchardt KL, Didier BT, Elsethagen T, Sun L, Gurumoorthi V, Chase J, Li J, Windus TL (2007) Basis set exchange: a community database for computational sciences. J Chem Inf Model 47 (3):1045–1052
20. Stevens WJ, Krauss M, Basch H, Jasien PG (1992) Relativistic compact effective potentials and efficient, shared-exponent basis sets for the third-, fourth-, and fifth-row atoms. Can J Chem 70:612–630
21. Becke AD (1993) Density functional thermochemistry. III. The role of exact exchange. J Chem Phys 98:5648–5652
22. Dobbs KD, Hehre WJ (1987) Molecular orbital theory of the properties of inorganic and organometallic compounds 5. Extended basis sets for first-row transition metals. J Comp Chem 6:861–879

23. Marchal B, Carbonniére P, Begue D, Pouchan C (2008) Structural and vibrational determination of small gallium–arsenide clusters from CCSD(T) and DFT calculations. Chem Phy Lett 453:49–54
24. Marchal R, Carbonnière P, Pouchan C (2012) Structural and vibrational properties prediction of SnnTen clusters (n = 2–8) using the GSAM approach. Comput Theoret Chem 990:100–105, In press
25. Bagno A, Bonchio M (2002) DFT calculations of 99Ru chemical shifts with all-electron and effective core potential basis sets. Eur J Inorg Chem. 1475–1483
26. Foster JP, Weinhold FJ (1980) Natural hybrid orbitals. Am Chem Soc 102:7211–7218
27. Glendening ED, Streitwieser AJ (1994) Natural energy decomposition analysis: an energy partitioning procedure for molecular interactions with application to weak hydrogen bonding, strong ionic, and moderate donor–acceptor interactions. Chem Phys 100:2900–2909
28. Reed AE, Curtiss LA, Weinhold F (1988) Intermolecular interactions from a natural bond orbital, donor-acceptor viewpoint. Chem Rev 88:899–926
29. Reed AE, Weinstock RB, Weinhold F (1985) Natural population analysis. J Chem Phys 83:735–745
30. Sebastian S, Sundaraganesan N (2010) The spectroscopic (FT-IR, FT-IR gas phase, FT-Raman and UV) and NBO analysis of 4-Hydroxypiperidine by density functional method. Spectrochim Acta Part A 75(3):941–952
31. Calhorda MJ, Lopes PEM (2000) An 'atoms in molecules' (AIM) analysis of the dihydrogen bond in organometallic compounds. J Organometal Chem 609:53–59
32. Bader RFW (1990) Atoms in molecules: a quantum theory. Oxford University Press, Oxford
33. Edgecombe KE, Esquivel RO, Smith VH Jr, Muller-Plathe F (2002) Pseudoatoms of the electron density. J Chem Phys 97:2593–2599
34. de Silva IC, de Silva RM, de Silva KMN (2005) Investigations of nonlinear optical (NLO) properties of Fe, Ru and Os organometallic complexes using high accuracy density functional theory (DFT) calculations. J Mol Struct Theochem 728:141–145
35. Mendesa PJ, Ramalho JPP, Candeias AJE, Robalod MP, Garcia MH (2005) Density functional theory calculations on h5-monocyclopentadienylnitrilecobalt complexes concerning their second-order nonlinear optical properties. J Mol Struct Theochem 729:109–113
36. Liyanage PS, de Silva RM, de Silva KMN (2003) Nonlinear optical (NLO) properties of novel organometallic complexes: high accuracy density functional theory (DFT) calculations. J MolStruc (Theochem) 639:195–201
37. Zeng T, Klobukowski M (2008) Relativistic model core potential study of the Au+Xe system. J Phys Chem A 112:5236–5242
38. Labello NP, Ferreira AM, Kurtz HA (2006) Utilizing relativistic effective core potentials for accurate calculations of molecular polarizabilities on transition metal compounds. J Phys Chem A 110:13507–13513
39. Gaur R, Mishra L (2012) Synthesis and characterization of Ru(II) −DMSO−Cl−chalcone complexes: DNA binding, nuclease, and topoisomerase II inhibitory activity. Inorg Chem 51:3059–3070
40. Stepanenko IN, Casini A, Edafe F, Novak MS, Arion VB, Dyson PJ, Jakupec MA, Keppler BK (2011) Conjugation of Organoruthenium(II) 3-(1H-Benzimidazol-2-yl)pyrazolo[3,4-b]pyridines and Indolo[3,2-d]benzazepines to recombinant human serum albumin: a strategy to enhance cytotoxicity in cancer cells. Inorg Chem 50:12669–12679
41. Tiana D (2009/2010) Organometallic chemistry from the interacting quantum atoms approach, Ph.D. Thesis, Università degli Studi di Milano, Milano, pp 18–19, 46
42. Farrugia LJ, Senn HM (2012) On the unusual weak intramolecular C…C interactions in $Ru_3(CO)_{12}$: a case of bond path artifacts introduced by the Multipole model? J Phys Chem A 116:738–746